On the Development of Coherent Structure in a Plane Jet*
(Part 1, Characteristics of Two-Point Velocity Correlation and Analysis of Eigenmodes by the KL Expansion)

Yasuhiko SAKAI**, Nobuhiko TANAKA** and Takehiro KUSHIDA**

The simultaneous measurement of the velocities at two points with X-type hot wire probes has been performed in three regions of a plane jet (i.e., the potential core region, the interaction region and the self-preserving region). The Karhunen Loève (KL) expansion was applied to the velocity data, and the development of coherent structure was investigated by the eigenvalues and eigenfunctions as well as the spatial velocity correlations. It is found that in the potential core region the first and second modes are dominant in the kinetic energy with almost the same magnitude. The profiles of the eigenfunctions downstream of the interaction region show that the first mode of streamwise velocity u is asymmetrical about the jet centerline whereas that of cross-streamwise velocity v is symmetrical. These results are consistent with the feature of the two-point velocity correlation.

Key Words: Jet, Turbulence, Vortex, Flow Measurements, Spatial Velocity Correlation, Karhunen Loève Expansion, Coherent Structure, Eigenvalue, Eigenfunction

1. Introduction

In recent years, the coherent structures in turbulent flows have been observed in many experiments and numerical simulations[1),(2)]. Since the coherent structures are closely related to drag, sound noise, mixing enhancement, vibration of solid structure, etc., the understanding of these physical characteristics is very important for industrial applications. In particular, from the viewpoint of the optimal design and the improvement of the fluid machinery, it is crucial to predict and control turbulent phenomena. However, the turbulent phenomena are very complicated and involved in various flow conditions, and so there seems to be no universal way of controlling them, and the method by trial and error is still necessary for each case. Therefore, the further investigation of the turbulent phenomena, in particular, the coherent structure is desired.

In this study, the plane jet is chosen as a research subject of the coherent structure. Since the jet is practically important and widely applied to various industrial fluid machineries, the fundamental characteristics have been studied by a lot of researchers[3),(4)]. However, the development of the coherent structure is essentially a nonlinear phenomenon, so that the dynamics is not clear and still an exciting subject for the researchers on turbulence. We applied the Karhunen Loève (KL) expansion which is also referred to as the Proper Orthogonal Decomposition (POD) to extract the coherent structures in turbulent fields. The POD, which is a non-conditional (objective) technique which is based on the two-point velocity correlation tensor, was proposed by Lumley (1967)[5] for the investigation of the coherent structures of inhomogeneous turbulent shear flows. Although there are some remarkable works on the jet flows using the KL expansion, the attention was put on the velocity field only at one downstream location or in the self-preserving region[6)-(9)]. In the authors' knowledge, there seems to be no studies in which over the wide range from a nozzle's exit to a sufficiently downstream region the development of the coherent structure was systematically investigated by means of the KL expansion. In this study, the KL expansion was applied to the data of two-point velocity correlation measured with the X-type hot wire probes, and the structure of the plane jet was investigated in three regions, i.e., the potential core region, the interaction region and the self-preserving region. In addition, to ascertain the fundamental features (the mean velocities, the turbulent intensities, the half-width, etc.) of the plane jet, one-point velocity measurements with one X-type hot wire probe were also

* Received 26th August, 2004 (No. 04-4193)

** Department of Mechanical Science and Engineering, Nagoya University, Furo-cho, Chikusa-ku, Nagoya 464–8603, Japan. E-mail: ysakai@mech.nagoya-u.ac.jp

carried out.

2. Karhunen-Loève Expansion

The KL expansion can extract the structure of the most energetic fluctuation in the random vector field[1]. In this study, the instantaneous velocity field $\boldsymbol{u}(x,t)$ was analyzed by the KL expansion. We explain the outline of the KL expansion for one component u of the velocity vector $\boldsymbol{u}$. The basis functions of the KL expansion $\phi_u(x)$ can be selected to maximize the normalized largest mean-square projection of u onto $\phi_u(x)$:

$$\max_{\phi_u} \frac{\left\langle |(\boldsymbol{u},\boldsymbol{\phi}_u)|^2 \right\rangle}{(\boldsymbol{\phi}_u,\boldsymbol{\phi}_u)}, \tag{1}$$

where $(\ ,\ )$ is defined as $(f,g)=\int_{\mathrm{I}} f(x)g(x)dx$ for any functions f, g in $\mathcal{L}^2$ space (I is a domain for applying the KL expansion.), $|\cdot|$ denotes the modulus, and $\langle\cdot\rangle$ is the ensemble average. This maximization process of the mean-square projection which is a classical problem in the calculus of variations leads to the following Fredholm integral eigenvalue equation[5]

$$\int_{\mathrm{I}} R_{uu}(x,x')\phi_u(x')dx' = \lambda_u \phi_u(x), \tag{2}$$

where the kernel is the two-point correlation function of velocity

$$R_{uu}(x,x') = \langle u(x)u(x') \rangle, \tag{3}$$

and λ_u and $\phi_u(x)$ denote the eigenvalue and the eigenfuction, respectively. Since $R_{uu}(x,x')$ is a positive definite symmetric function, the Hilbert-Schmidt theory assures us that there is a countable infinity of eigenvalues and eigenfunctions that provides a diagonal decomposition:

$$R_{uu}(x,x') = \sum_{n=1}^{\infty} \lambda_u^{(n)} \phi_u^{(n)}(x)\phi_u^{(n)}(x'). \tag{4}$$

The Hilbert-Schmidt theory provides a series of properties for the eigenvalues and the eigenfunctions.

(a) There exists a countable set of discrete solutions to Eq. (2) (The eigenfunction $\phi_u^{(n)}$ corresponds to the eigenvalue $\lambda_u^{(n)}$).

$$\int_{\mathrm{I}} R_{uu}(x,x')\phi_u^{(n)}(x')dx' = \lambda_u^{(n)} \phi_u^{(n)}(x), \tag{5}$$

(b) The eigenvalues are real, and those are usually arranged in order of magnitude

$$\lambda_u^{(1)} > \lambda_u^{(2)} > \lambda_u^{(3)} \cdots. \tag{6}$$

(c) The eigenfunctions are orthogonal and can be normalized so that

$$\int_{\mathrm{I}} \phi_u^{(n)}(x)\phi_u^{(m)}(x)dx = \delta_{nm}. \tag{7}$$

(d) The velocity field can be expressed as a linear combination of the eigenfunctions

$$u(x,t) = \sum_{n=1}^{\infty} a_u^{(n)}(t)\phi_u^{(n)}(x), \tag{8}$$

where from the orthogonality of the eigenfunctions the random coefficients $a_u^{(n)}(t)$ is obtained as follows

$$a_u^{(n)}(t) = \int_{\mathrm{I}} u(x)\phi_u^{(n)}(x)dx. \tag{9}$$

$$\left\langle a_u^{(n)} a_u^{(m)} \right\rangle = \lambda_u^{(m)} \delta_{nm}. \tag{10}$$

The KL expansion (POD) is literally Eq. (8).

(e) The integral of the mean square value of the fluctuating velocity u in the domain I is given by the sum of the eigenvalues,

$$E_u = \int_{\mathrm{I}} \left\langle u^2(x,t) \right\rangle dx = \sum_{n=1}^{\infty} \lambda_u^{(n)}. \tag{11}$$

Since the eigenvalues are arranged in order of magnitude (see Eq. (6)), the first eigenvalue contains the largest amount of the turbulent kinetic energy. From this reason, Lumley[10] suggested that the first (or first a few low-order) eigenfunction(s) (i.e., mode(s)) represents the coherent structure if it contains a dominant percentage of the turbulent kinetic energy.

In the actual measurements, x is chosen as the discrete spatial points. Then Eq. (5) can be described as the following eigenvalue ploblem of the correlation tensor

$$\sum_{j=1}^{N} R_{uu}(x^{(i)},x^{(j)})w(x^{(j)})\boldsymbol{\phi}_u^{(n)}(x^{(j)})\Delta x = \lambda_u^{(n)} \boldsymbol{\phi}_u^{(n)}(x^{(i)}), \tag{12}$$

where Δx is the spacing between neighbor measuring points, N is the number of measuring positions, and $w(x^{(j)})$ is the weigthing function[8]

$$w(x^{(j)}) = [0.5, \overbrace{1,1,\cdots,1}^{N-2}, 0.5]^T. \tag{13}$$

Here it should be noticed that the sign of eigenfunction $\boldsymbol{\phi}_u^{(n)}$ can not be determined because the Eq. (12) is true for both $\boldsymbol{\phi}_u^{(n)}$ and $-\boldsymbol{\phi}_u^{(n)}$.

3. Experimental Methods and Conditions

Figure 1 shows the schematic of experimental apparatus near the nozzle exit and the coordinate system. The skimmer was installed at the position of about 1 mm downstream from the nozzle exit to eliminate the boundary layer which develops along the contraction wall. The height d and the width l of the skimmer exit are 12 mm and 236 mm, respectively. The velocity U_0 at the skimmer exit is about 20 m/s, and Reynolds number $Re(=U_0 d/\nu)$ is about 16 000. Further, the sidewall was set vertically at the test section to inhibit the entrainment from the surrounding. With the use of the skimmer and the sidewall, the uniform velocity profile at the skimmer exit and a good 2-dimensional flow field at the test section could be realized. The coordinate system is as follows: the axial (streamwise) coordinate is x_1, the vertical (cross-streamwise) coordinate is x_2 and the spanwise coordinate is x_3. The simultaneous measurements of two-point velocities were

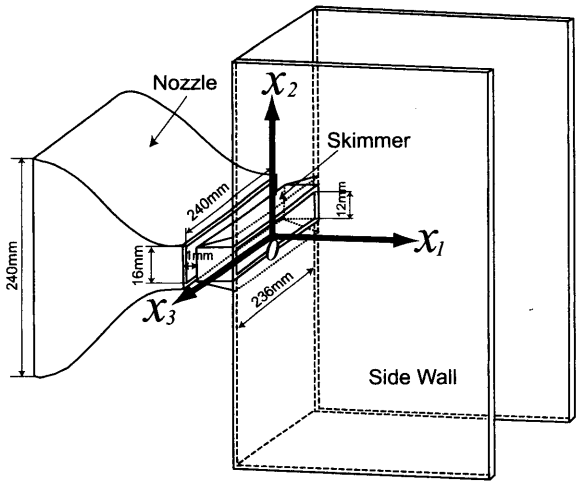

Fig. 1 Schematic of the experimental apparatus near the nozzle exit and the coordinate system

carried out at six downstream locations, i.e., $x_1/d = 2.0$, 3.0 (in the potential core region), $x_1/d = 4.5$ (in the early stage of the interaction region), $x_1/d = 6.0$ (in the late stage of the interaction region) and $x_1/d = 10.0$, 20.0 (in the self-preserving region). The 21 points at each downstream location are selected, so that the number of terms in the KL expansion is 21. The interval Δx of neighbor measuring points is adjusted to $2.5b/10$ (b: the half-width of the axial mean velocity) at each downstream location. The integral kernel of the KL expansion is the two-point correlation tensor $R_{\alpha\alpha}(x_2, x_2') = \langle \alpha(x_2)\alpha(x_2') \rangle$, where α denotes either u or v; u is the axial (x_1-directional) velocity and v is the vertical (x_2-directional) velocity. Since $R_{\alpha\alpha}(x_2, x_2') = R_{\alpha\alpha}(x_2', x_2)$, and $R_{\alpha\alpha}(x_2, x_2)$ is obtained with one probe, the total combination number of measurements is ${}_N C_2$ when the number of measuring points is N at each downstream location. In the experiment, N is 21, and so the total number of measurements is ${}_{21}C_2 = 210$.

4. Fundamental Properties

To examine the fundamental properties of the present plane jet, firstly, the one-point velocity measurements were carried out with one X-type hot wire probe before the two-point measurements. In this section, the results are described.

Figure 2 shows the axial variation of the centerline mean streamwise velocity U_m. It is known that the variation obeys the $-1/2$ power law in the self-preserving region of the plane jet[3]. From Fig. 2, it is found that the $-1/2$ power law is applicable at $x_1/d \geq 6.0$. The least squares approximation of $(U_m/U_0)^{-2}$ at $x_1/d \geq 6.0$ gives the solid line in Fig. 2,

$$\left(\frac{U_m}{U_0}\right)^{-2} = 0.134\left(\frac{x_1}{d} + 3.41\right). \tag{14}$$

Further, although the vertical profile of the axial mean velocity U is not presented here, we confirmed that it agrees very well with the Gaussian distribution.

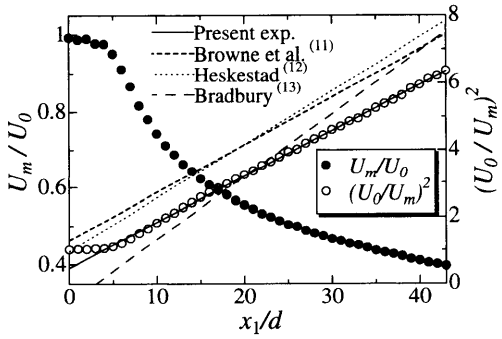

Fig. 2 Axial variation of centerline mean streamwise velocity U_m

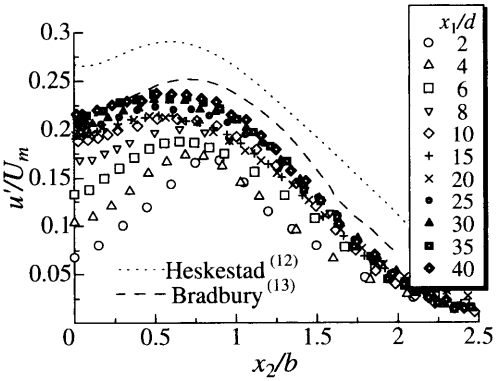

Fig. 3 The cross-streamwise profiles of u'

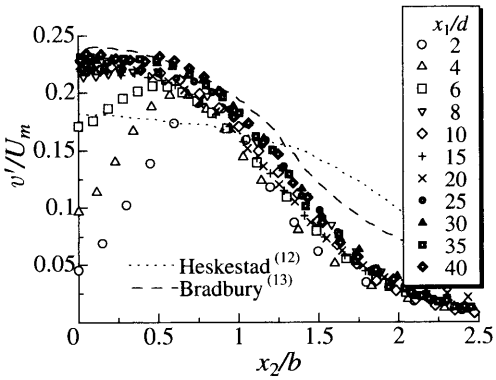

Fig. 4 The cross-streamwise profiles of v'

Figures 3 and 4 present the vertical profiles of the r.m.s. values u' and v' of axial and vertical velocity fluctuations, respectively. Both profiles show a good similarity at $x_1/d > 10.0$. In the profiles of u', the peaks appear in both sides of the jet centerline at all downstream locations, whereas in the profiles of v' the peaks can not be observed clearly at $x_1/d > 10.0$, but at $x_1/d \leq 6.0$ the peaks in both sides of the jet centerline exist as in the profiles of u'. Figure 5 presents the profiles of the Reynolds stress. The ordinate is normalized by U_m^2. The profiles show similarity at $x_1/d > 8.0$, and the peak is located at $0.6 < x_2/b < 0.7$.

Figure 6 presents the streamwise variation of the half-

width b of the streamwise mean velocity. Both the abscissa and the ordinate are normalized by the skimmer height d. In the self-preserving region, it is known that the half width spreads linearly with x_1[3]. The data at $x_1/d \geq 6.0$ are approximated well by the following equation,

$$\frac{b}{d} = 0.108\left(\frac{x_1}{d} + 2.63\right), \tag{15}$$

which is shown in Fig. 6 by the solid line. From the figure, it is also found that the spreading rate agrees well with the results of other researchers except for the result of Bradbury[13]. Here it is noted that the result of Bradbury[13] should not be simply compared with the others, because in his experiment the jet was issued into the main stream with $0.16U_0$. In the case, it is known that the spread of the plane jet becomes narrower than that of jet issued into a stationary fluid[13]. Further, it was confirmed that the mean velocity, the r.m.s. values of velocity fluctuations and the Reynolds stress are uniform in the region $-3.0 \leq x_3/d \leq 3.0$. Therefore the present plane jet has a good 2-dimensionality despite the low aspect ratio of skimmer exit (which is 19.7 in this experiment).

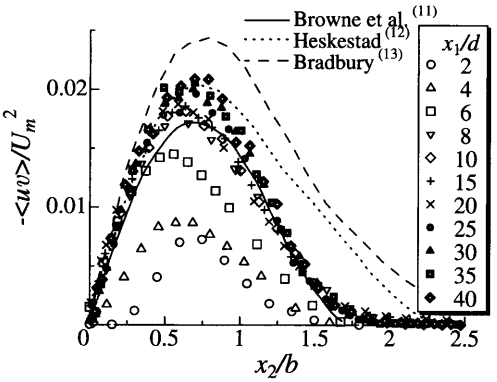

Fig. 5 The cross-streamwise profiles of $-\langle uv\rangle$

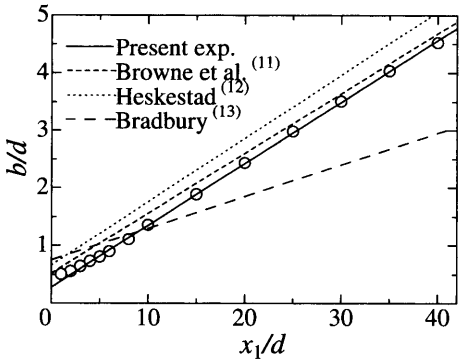

Fig. 6 Streamwise variation of the half-width b

5. Results of the Two-Point Measurements

The simultaneous measurements of the velocities at two points with the X-type hot wire probes have been performed in three regions of the plane jet. The two-point spatial velocity correlation and the results by the KL expansion analysis are described in this section.

5.1 Mean velocity and r.m.s. velocity by the two-point measurements

Figures 7–9 show the profiles of the mean velocity U and the r.m.s. values u' and v' to confirm the reliability of the simultaneous measurements at two points. The measurements were performed at $x_1/d = 2.0, 4.5, 6.0, 10.0$ and 20.0, but only the results at $x_1/d = 2.0$ and 20.0 are shown in the figures. The data with two probes (which are denoted by probe 1 and probe 2 in the figures) agrees very well with each other. It was also confirmed that there was almost no significant drop of the output of hot-wire anemometer through the measuring time. Further, from the comparison of Figs. 8 and 9 with Figs. 3 and 4, the data of the two-point measurements agree very well with those of one-point measurements at $x_1/d = 2.0$, 20.0. Therefore we concluded that the present simultaneous measurements at two points with the X-type hot wire probes are sufficiently reliable.

5.2 Two-point spatial velocity correlation

One of the most important statistics obtained by the simultaneous measurement at two points is the two-point spatial velocity correlation. The two-point spatial velocity correlation[14] is defined by

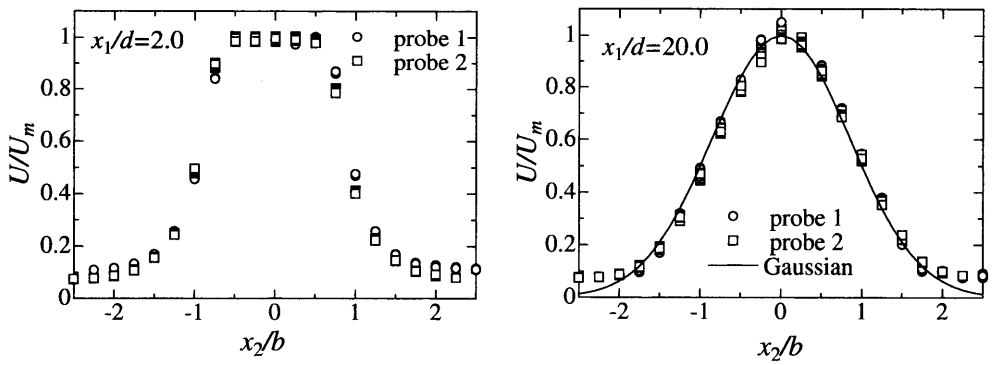

Fig. 7 The profiles of the streamwise mean velocity U for the two-point measurements

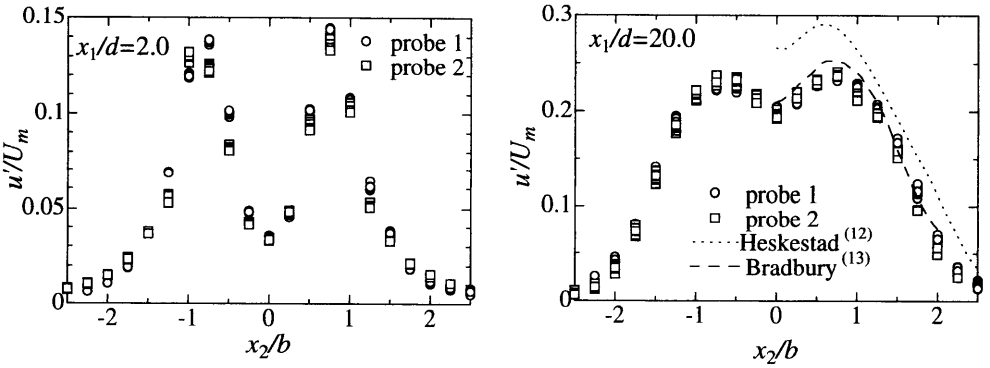

Fig. 8 The profiles of the r.m.s. values of the streamwise velocity u' for the two-point measurements

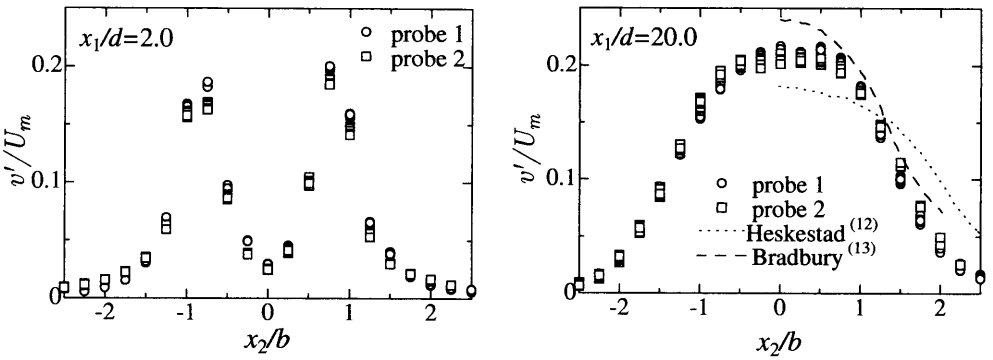

Fig. 9 The profiles of the r.m.s. values of the cross-streamwise velocity v' for the two-point measurements

$$C_{\alpha\alpha}(x_2,x_2')=\frac{\langle\alpha(x_2,t)\alpha(x_2',t)\rangle}{\sqrt{\langle\alpha^2(x_2,t)\rangle}\sqrt{\langle\alpha^2(x_2',t)\rangle}}, \qquad (16)$$

where α denotes either u or v. The value of $C_{\alpha\alpha}$ is in the range $[-1.0,+1.0]$. Since $C_{\alpha\alpha}$ corresponds to the dimensionless quantity of $R_{\alpha\alpha}(x,x')$ which is the integral kernel of the KL expansion, the investigation of the feature of the $C_{\alpha\alpha}$ profile is useful in considering the results of the KL expansion which is given in section 5.3. Figure 10 (a) – (c) present the downstream variations of the spatial correlation coefficient C_{uu} and C_{vv} at $x_1/d = 2.0$, 4.5 and 20.0. The contours in these figures are drawn at the increment of 0.1; the solid line denotes a positive value (or zero) and the broken line denotes a negative value. It is noted that $C_{uu} = C_{vv} = 1.0$ at $x_2/b = x_2'/b$ which corresponds to the probe's position. From the profiles of the mean velocity and the r.m.s. velocity explained in section 3, $x_1/d = 2.0$ and 3.0 are in the potential core region, $x_1/d = 4.5$ and 6.0 are in the interaction region and $x_1/d = 10.0$ and 20.0 are in the self-preserving region. Here, $x_1/d = 2.0$, 4.5 and 20.0 are selected as the representative for each region. From Fig. 10, it is found that the feature of the contours is different in each region. Therefore it is expected that the eigenvalues and the eigenfunctions of the KL expansion also show the different features in each region.

Here we pay attention to the symmetric positions with respect to the jet centerline (corresponding to the second and fourth quadrant in Fig. 10). In the second and fourth quadrant, C_{uu} is positive and C_{vv} is negative in the potential core region ($x_1/d = 2.0$), both correlations are almost zero in the interaction region ($x_1/d = 4.5$), and C_{uu} is negative and C_{vv} is positive in the self-preserving region ($x_1/d = 20.0$). In particular, the negative correlation of C_{uu} in the self-preserving region may be caused by the self-preserving antisymmetric array of counter-rotating vortices reported in many other researchers[15]–[17]. This feature is considered to be the appearance of the 'flapping' phenomenon[15] suggested as one of the large scale structures in the turbulent plane jet. On the other hand, the signs of C_{uu} and C_{vv} in the potential core region are just inverse to those in the self-preserving region, and this feature can be explained by the fact that the counter-rotating vortices are formed symmetrically with respect to the jet centerline. The phenomenon with the positive correlation between streamwise fluctuating velocity on opposite sides of the jet centerline is called the 'puffing'[15]. Further, from the almost zero correlation in the interaction region, it is considered that the symmetric vortices in the potential core region have collapsed due to the interaction of the mixing layers.

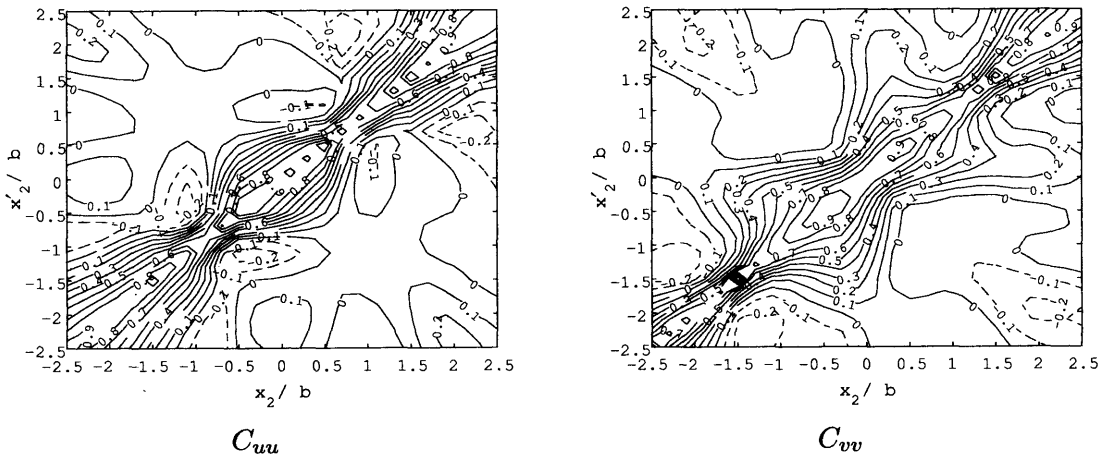

(a) $x_1/d = 2.0$ (in the potential core region)

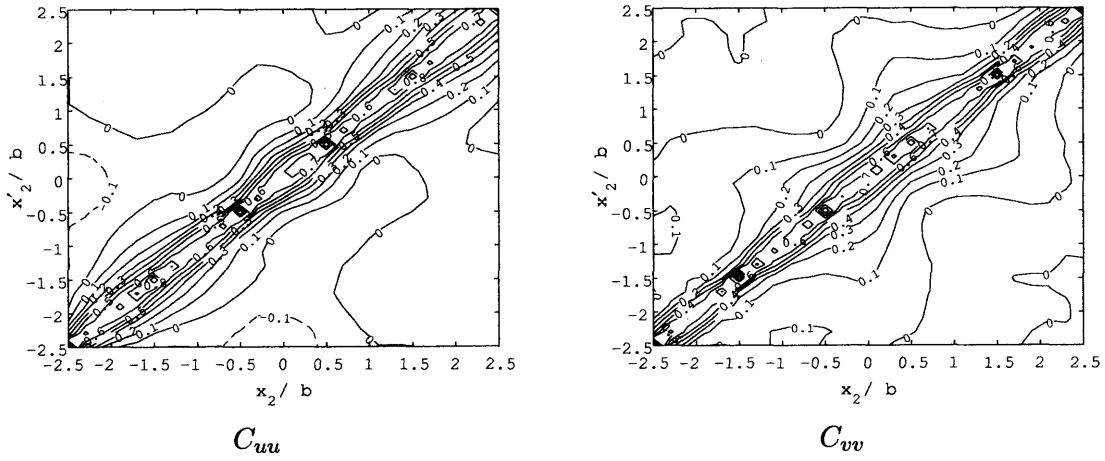

(b) $x_1/d = 4.5$ (in the interaction region)

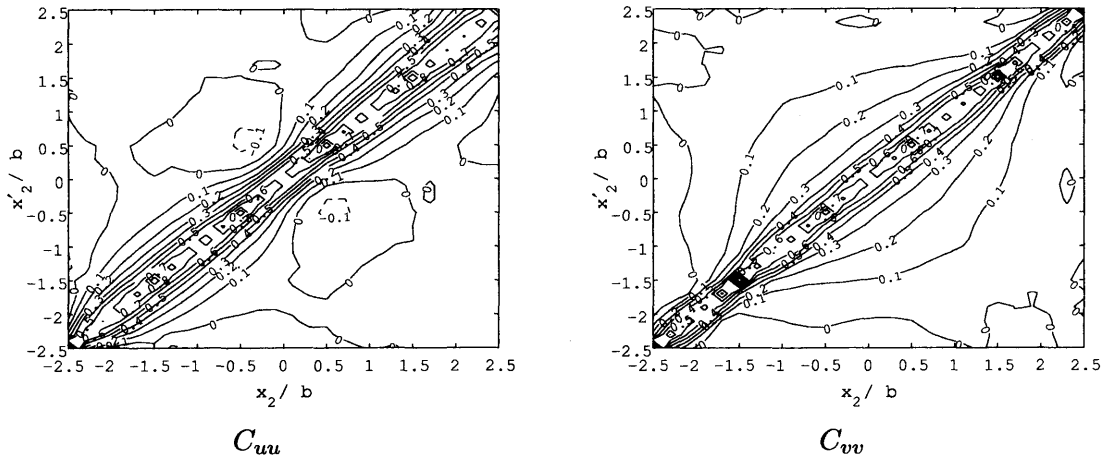

(c) $x_1/d = 20.0$ (in the self-preserving region)

Fig. 10 The downstream variations of the spatial correlation coefficient C_{uu}, C_{vv}

5.3 Results by the KL expansion

5.3.1 Eigenvalues Figure 11 (a) and (b) present the downstream variations of the distributions of eigenvalues $\lambda_u^{(n)}$ and $\lambda_v^{(n)}$. The ordinate is normalized by the integral E_u (or E_v) of the mean square value of the fluctuating velocity (see Eq. (11)), and the abscissa denotes the number of terms of the KL expansion. The number of measurement points at each downstream location are 21, and consequently the number of terms of the KL expansion is 21. E_u and E_v are also given by the sum of all eigenvalues: $E_u = \sum_{n=1}^{21} \lambda_u^{(n)}$ and $E_v = \sum_{n=1}^{21} \lambda_v^{(n)}$. Consequently the value

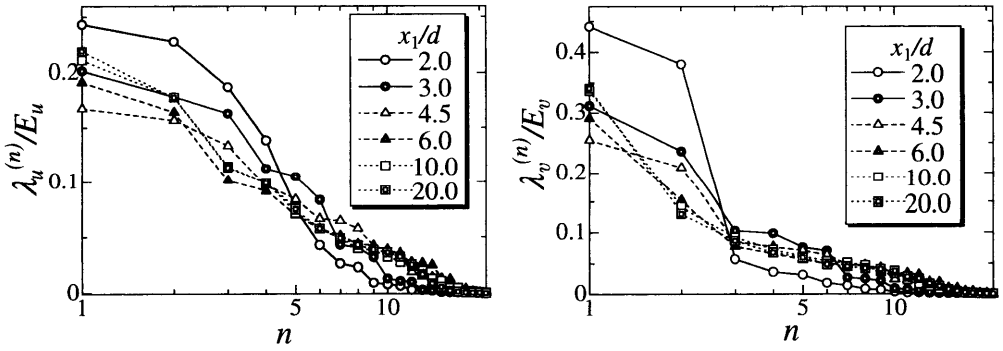

(a) u-eigenvalue (b) v-eigenvalue

Fig. 11 The downstream variation of the eigenvalue $\lambda_u^{(n)}$, $\lambda_v^{(n)}$

of the ordinate means the contribution of each mode to the sum of all eigenvalues. From Fig. 11 (a) and (b), the distributions at $x_1/d = 10.0$ and 20.0 agree very well with each other, but the distributions at $x_1/d = 2.0$, 3.0, 4.5 and 6.0 show different shapes.

Firstly, we pay attention to the change of the distribution from $x_1/d = 2.0$ to 4.5. In the stage from $x_1/d = 2.0$ to 3.0, as for the distribution of u-eigenvalue, the contributions of first four modes decrease and the contributions over the fourth mode increase. As for the v-eigenvalue, the contributions of first two modes decrease and the contributions over the second mode increase. In the stage from $x_1/d = 3.0$ to 4.5, as for both u and v-eigenvalue, the contributions of first six modes decrease and the contributions over the sixth mode increase. From the results, it is considered that the vortex structures which contain large energy (i.e., lower-order terms) collapse and the energy is transferred to the small scale vortex structures with small energy (i.e., higher-order terms). In the distributions of u and v-eigenvalue at $x_1/d = 2.0$, both contributions of the first and second mode are very large and their magnitudes are almost the same. Therefore it is naturally considered that the first and second modes in the potential core region correspond to the symmetric vortices near an nozzle exit.

Secondly, the change of distributions from $x_1/d = 4.5$ to 10.0 is discussed. In this region, the contributions of lower-order terms increase. This result suggests that after the collapse of vortex structures in the potential core region the reconstruction of vortex structures proceeds and the structures with large energy are produced again.

Finally, in the region from $x_1/d = 10.0$ to 20.0, i.e., in the self-preserving region, it is expected that the stable structures are formed because the shapes of profiles at $x_1/d = 10.0$ and 20.0 agree very well with each other.

Further, from the comparison of the distributions of $\lambda_u^{(n)}$ and $\lambda_v^{(n)}$, it is found that the contribution of the first v-mode $\lambda_v^{(1)}$ is larger than that of the first u-mode $\lambda_u^{(1)}$ in all regions, and in particular $\lambda_v^{(1)}$ is more than twice as large as that of the second v-mode $\lambda_v^{(2)}$ in the self-preserving region. This result means that the first v-mode $\phi_v^{(1)}$ influences dominantly on the fluctuating cross-streamwise velocity field.

5.3.2 Eigenfunctions Figure 12 (a) – (f) present the downstream variations of the first and second eigenfunctions $\phi_u^{(1)}(x_2)$, $\phi_u^{(2)}(x_2)$, $\phi_v^{(1)}(x_2)$ and $\phi_v^{(2)}(x_2)$. As discribed in section 2, the eigenfunction is normalized by Eq. (7). ($\phi_v^{(n)}(x_2)$ is also expressed as the same manner as Eq. (7).) Again it should be noticed that the sign of eigenfunctions $\boldsymbol{\phi}_u^{(n)}$ (or $\boldsymbol{\phi}_v^{(n)}$) can not be determined. Since the eigenfunction changes very much upstream and downstream of $x_1/d = 3.0$, we first consider at $x_1/d \geq 3.0$. At $x_1/d \geq 4.5$, the shape of the first u-mode $\phi_u^{(1)}(x_2)$ is like a sine curve. This shape has the effect of acceleration at one side of the jet flow field and deceleration at another side. Therefore the first u-mode $\phi_u^{(1)}(x_2)$ has the effect to make the streamwise correlation C_{uu} negative on opposite sides of the jet centerline. This is consistent with the 'flapping'[15] phenomenon which is a characteristic of the structure in the self-preserving region explained in section 5.2. It is also understood that the feature of the negative C_{uu} on opposite sides of the jet centerline is due to the most energetic structure in the self-preserving region, i.e., the first mode of the KL expansion.

As for the v-mode ϕ_v, it is found that the second v-mode $\phi_v^{(2)}$ has an asymmetric shape similar to that of the first u-mode $\phi_u^{(1)}$, but the first v-mode $\phi_v^{(1)}$ shows a symmetric shape with respect to the jet centerline ($x_2/b = 0$). It is noticed that the change of $\phi_v^{(1)}$ at $x_1/d \geq 4.5$ is similar to that of v' (see Fig. 4, i.e., the profile of v' has peaks in both sides of the jet centerline at $x_1/d \leq 6.0$ and has one peak near the centerline at $x_1/d \geq 10.0$). This shape of $\phi_v^{(1)}$ has the same effect on the velocity field for both sides of the jet (i.e., if the flow is accelerated (decelerated) at one side of the jet flow field, then the flow at another side is also accelerated (decelerated)), and the cross-streamwise correlation C_{vv} becomes positive on opposite sides of the jet centerline. This result agrees with the feature of C_{vv} in the self-preserving region as discussed in section 4.2. Further, it is noted that the shape of the second u-mode $\phi_u^{(2)}$ is similar to that of u' (see Fig. 3).

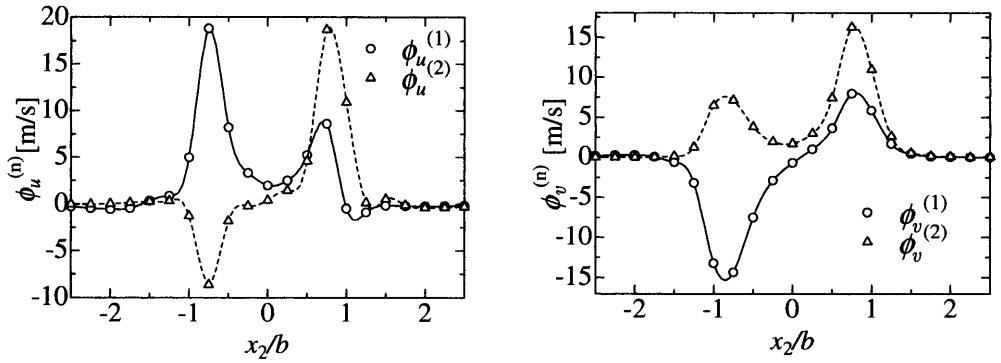

(a) $x_1/d = 2.0$

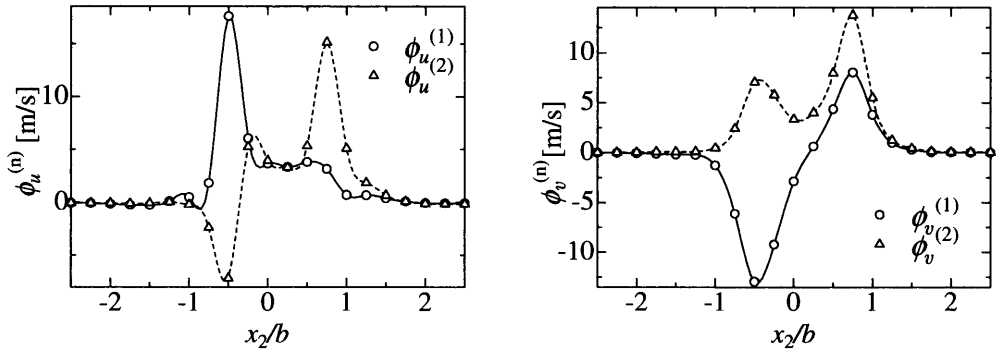

(b) $x_1/d = 3.0$

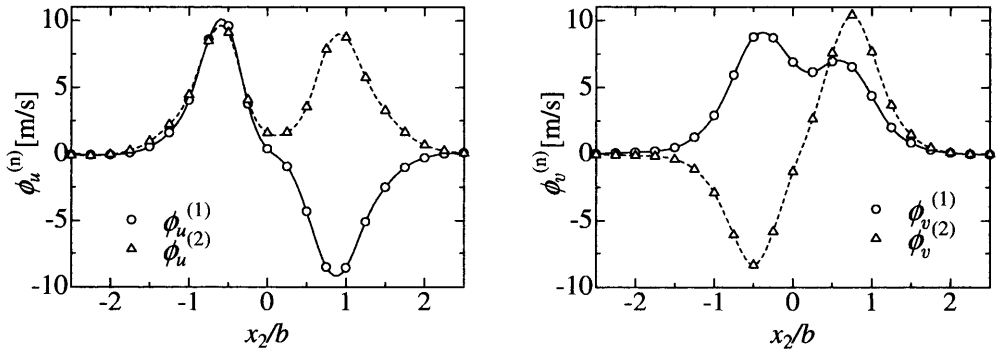

(c) $x_1/d = 4.5$

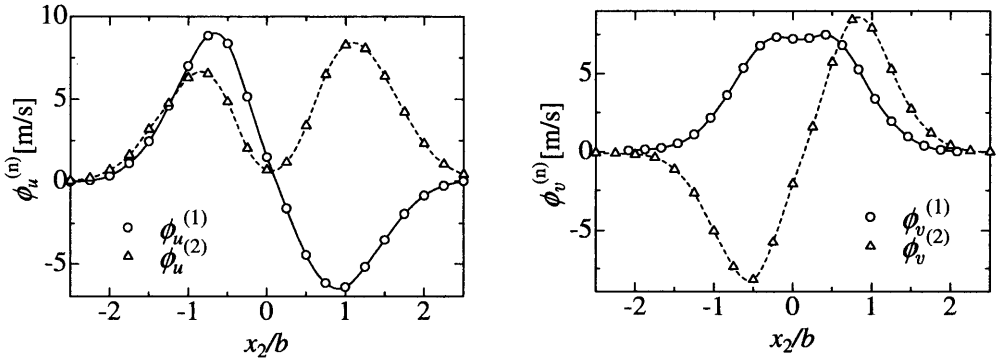

(d) $x_1/d = 6.0$

Fig. 12 (to be continued)

Next we consider the potential core region (x_1/d = 2.0, 3.0). At $x_1/d = 2.0$, both profiles of the first and second mode for each of u and v components have a large peak only in one side. Since the energy contributions of the first and second mode for each of u and v components are almost of the same magnitude (see Fig. 11), it is expected that the symmetric vortices are emitted from the nozzle exit.

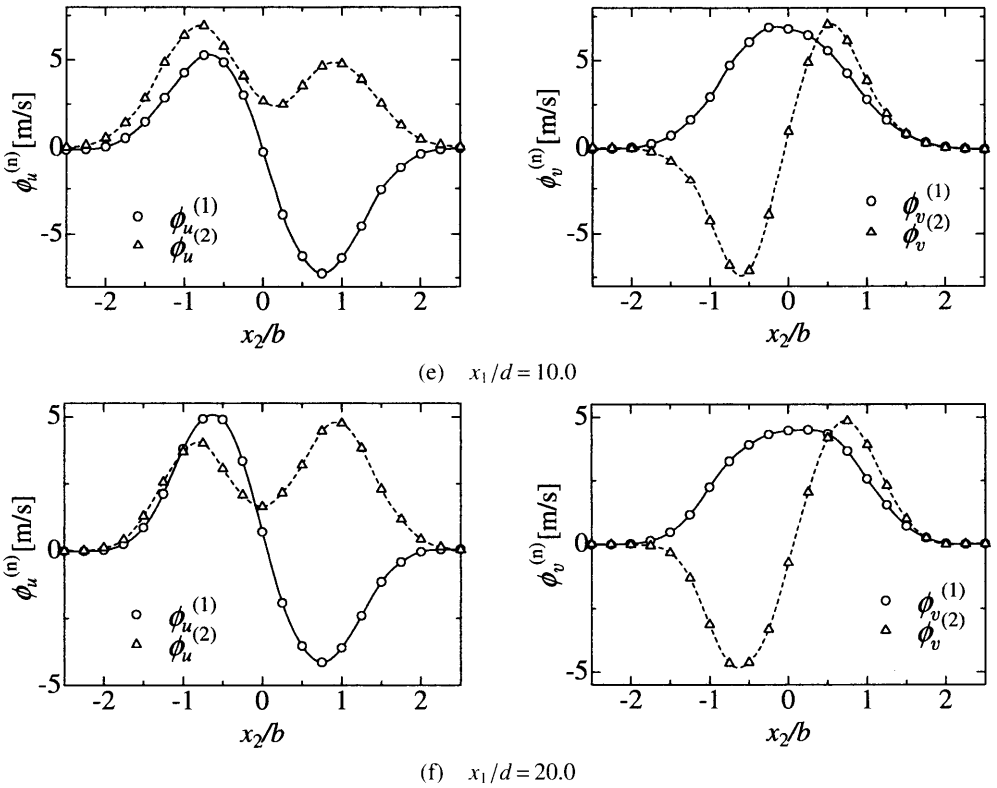

Fig. 12 The downstream variations of the eigenfunctions $\phi_u^{(n)}$, $\phi_v^{(n)}$

6. Conclusions

The simultaneous measurements at two points with the X-type hot wire probes were preformed in three regions of the turbulent plane jet, and the development of the coherent structure was investigated focusing on mainly the two-point spatial correlations, eigenvalues and eigenfunctions of the KL expansion.

(1) On the two-point spatial velocity correlations:
On opposite sides of the jet centerline, C_{uu} is positive and C_{vv} is negative in the potential core region, both are almost zero in the interaction region, and C_{uu} is negative and C_{vv} is positive in the self-preserving region.

(2) On the KL expansion:
(2-1) Eigenvalues:
(a) In the potential core region, the energy contributions of the first and second modes for each of u and v components are very large and their magnitudes are almost of the same value.
(b) The contribution of the first v-mode is larger than that of the first u-mode in all regions, and the contribution of the first v-mode is more than twice as large as that of the second v-mode in the self-preserving region.
(2-2) Eigenfunctions:
(a) In the interaction and self-preserving regions, the first u-mode shows an antisymmetric profile and the first v-mode a symmetric profile. These shapes are consistent with the feature of the spatial correlations on opposite sides of the jet centerline.
(b) In the potential core region, the profiles of the first and second modes for each of u and v components have large peaks only on one side of the jet centerline. Since the contributions of the energy of the first and second modes are almost of the same magnitude, it is considered that the symmetric vortices are issued from the nozzle exit.

References

(1) Holmes, P., Lumley, J.L. and Berkooz, G., Turbulence, Coherent Structures, Dynamical Systems and Symmetry, (1996), pp.86–128, Cambridge Univ. Press.
(2) Da Silva, C.B. and Mètatis, O., On the Influence of Coherent Structures upon Interscale Interactions in Turbulent Plane Jet, J. Fluid Mech., Vol.473 (2002), pp.103–145.
(3) Rajaratnum, N., Turbulent Jets, (1976), pp.1–25, Elsevier Scientific Publishing Company.
(4) Gutmark, E. and Wygnanski, I., The Planar Turbulent Jet, J. Fluid Mech., Vol.73 (1976), pp.465–495.
(5) Lumley, J.L., The Structure of Inhomogeneous Turbulent Flows, Atmospheric Turbulence and Radio Wave Propagation, Edited by Yaglom, A.M. and Tatarsky, V.I., (1967), pp.166–178, Nauka, Moscow.
(6) Delville, J., Ukeiley, L., Cordier, L. and Bonet, J.P., Examination of Large Scale Structures in a Plane Mixing Layer, J. Fluid Mech., Vol.391 (1999), pp.91–112.
(7) Citrinniti, J.H. and George, W.K., Reconstruction of the Global Velocity Field in the Axisymmetric Mixing

Layer Utilizing the Proper Orthogonal Decomposition, J. Fluid Mech., Vol.418 (2000), pp.137–166.

(8) Gordeyev, S.V. and Thomas, F.O., Coherent Structure in the Turbulent Planner Jet. Part 1. Extraction of Proper Orthogonal Decomposition Eigenmodes and Their Self-Similarity, J. Fluid Mech., Vol.414 (2000), pp.145–194.

(9) Gordeyev, S.V. and Thomas, F.O., Coherent Structure in the Turbulent Planner Jet. Part 2. Structual Topology via POD Eigenmode Projection, J. Fluid Mech., Vol.460 (2002), pp.349–380.

(10) Lumley, J.L., Transition and Turbulence, Edited by Meyer, R.E., (1981), pp.215–241, Academic.

(11) Browne, L.W.B., Antonia, R.A. and Rajagopalan, S., Interaction Region of a Two-Dimensional Turbulent Plane Jet in Still Air, Structure of Complex Turbulent Shear Flows, Edited by Dumus, R. and Fulachier, L., (1983), pp.189–196.

(12) Heskestad, G., Hot-Wire Measurements in a Plane Turbulent Jet, J. Appl. Mech, Vol.32 (1965), pp.721–734.

(13) Bradbury, L.J.S., The Structure of a Self-Preserving Turbulent Plane Jet, J. Fluid Mech., Vol.23, Part 1 (1965), pp.31–64.

(14) Hino, M., Spectrum Analysis, (in Japanese), (1977), pp.52–55, Asakura Press.

(15) Goldschmidt, V.W. and Bradshow, P., Flapping of a Plane Jet, Phys. Fluids, Vol.16, No.3 (1973), pp.354–355.

(16) Cervantes de Gortari, J. and Goldschmidt, V.W., The Apparent Flapping Motion of a Turbulent Plane Jet-Further Experimental Results, J. Fluid Eng., Vol.103 (1981), pp.119–126.

(17) Antonia, R.A., Chambers, A.J., Britz, D. and Browne, L.W.B., Organized Structures in a Turbulent Plane Jet, J. Fluid. Mech., Vol.134 (1983), pp.49–66.